Springer

KSME

Journal of Mechanical Science and Technology 32 (9) (2018) 4299~4312
www.springerlink.com/content/1738-494x(Print)/1976-3824(Online)
DOI 10.1007/s12206-018-0828-y

Modeling of dynamic recrystallization in white layer in dry hard cutting by finite element—cellular automaton method †

Duan Chunzheng*, Zhang Fangyuan, Qin Siwei, Sun Wei and Wang Minjie

School of Mechanical Engineering, Dalian University of Technology, Dalian 116024, China

(Manuscript Received August 6, 2017; Revised April 11, 2018; Accepted May 23, 2018)

Abstract

White layer formed in hard cutting process has great influence on surface quality of the workpiece, simulation of the white layer has great significance. Dynamic recrystallization critical temperature model is derived to calculate the critical temperature of the dynamic recrystallization in the white layer. A finite element model was developed to simulate the hard cutting process based on the Johnson-Cook constitutive equation. The dynamic recrystallization critical temperature was derived based on the true stress-strain curves obtained by the split Hopkinson pressure bar experiments. The cellular automaton model which aims to simulate the white layer grains formed by the dynamic recrystallization process in hard cutting is established. The temperature and strain data extracted from the finite element model are used in the cellular automaton model. The contrast between the simulation and experimental results demonstrates that the cellular automaton model can simulate the dynamic recrystallization process in the white layer accurately. The dynamic recrystallization processes in the white layer under different cutting speed and flank wear are simulated based on the finite element - cellular automaton model. The results show that the dynamic recrystallization grain size of the white layer decreases with the increase in cutting speed and tool wear.

Keywords: Dry hard cutting; Dynamic recrystallization; Finite element model; Cellular automaton model; White layer

1. Introduction

Dry hard cutting is widely used in machining of hardened steel owing to its low cost, high machining efficiency and green environmental protection. The cutting mechanism of the dry hard cutting is different from that of traditional cutting because of multi field coupling effect in the dry hard cutting process. Therefore, the formation mechanism and evolution law of the microstructure of cutting deformation zone have become one of the key problems in dry hard cutting [1]. Numerous studies have shown that the white layer can be observed in the machined surface of dry hard cutting. The white layer determines the distribution of the stress, strain and the physical as well as mechanical properties of the machined surface, which has great influence on workpiece performance [2, 3].

Some scholars have studied the formation mechanism of the white layer, the dynamic recrystallization mechanism and phase transformation mechanism are considered as two main formation mechanisms of the white layer. The scholars who support the dynamic recrystallization mechanism believe that plastic deformation plays a role in the formation of the white layer, plastic deformation in the machined surface leads to sharp increase in dislocation density and temperature in the machined surface, the dynamic recrystallization is easier to occur under high temperature and high dislocation density. Moreover, the strain energy produced by plastic deformation can provide driving force for dynamic recrystallization nucleation. The rapid nucleation and growth processes of the dynamic recrystallization grains lead to the formation of the white layer [4-6]. The scholars who propose the phase transformation mechanism consider that the high temperature produced by the cutting process can cause austenitizing in the machined surface, and martensite phase transformation occurs as the result of rapid cooling rate when the tool leaves the machined surface, the white layer is formed during the rapid phase transformation process [7, 8]. However, Bosheh and Mativenga [9] found that the white layer can also be observed when the temperature in the machined surface is lower than austenite transformation temperature. Some researchers consider that the white layer is formed by plastic deformation - phase transformation mechanism. Hosseini et al. [10] made research on the white layer through cutting AISI52100 steel under high cutting speed, they concluded that the white layer is formed by the plastic deformation mechanism when the

*Corresponding author. Tel.: +86 18041180978, Fax.: +86 41184708742
E-mail address: duancz@dlut.edu.cn
† Recommended by Associate Editor In-Ha Sung

cutting temperature is lower than phase transformation temperature, while the white layer is formed by the phase transformation mechanism when the cutting temperature is higher than phase transformation temperature.

The formation of the white layer under different cutting parameters was studied as well. Akcan and Shahs [11] reported that the white layer thickness increases with cutting speed in a certain range through studying the high speed cutting of AISI52100 hardened steel. Attanasio and Umbrello [12] observed the white layer produced in hard cutting of AISI 52100 steel, the results indicated that the flank wear VB has influence on the white layer formation, the white layer thickness increases with flank wear.

Some researchers have also attempted to establish the simulation model of the white layer. Chou and Song [13] established the temperature field in the machined surface based on Jaeger moving heat source model and estimated the white layer thickness according to the critical temperature of martensite phase transformation. Ambrogio et al. [14] proposed a prediction model for white layer thickness through response surface methodology. Umbrello et al. [15, 16] established a finite element (FE) model based on the constitutive equation which contains hardness variable, the white layer thickness of AISI52100 steel was simulated using this model. Ramesh et al. [17, 18] used the modified critical austenite transformation temperature as the critical criterion of the white layer formation and established the FE model of the white layer thickness.

Most of the previous models focus on the simulation and prediction of the white layer thickness, but the study on the dynamic evolution process of the microstructure in the white layer formation process has not been reported. The grain size in the white layer directly determines the micro strain and hardness of the machined surface, which has great influence on the surface quality and workpiece performance. The FE model is good at simulating material's macroscopic thermodynamic behavior, such as the temperature field, the stress and strain fields. However, the FE method is not good at simulating the microscopic behavior of the material. Several approaches such as cellular automaton (CA) method, Monte Carlo (MC) method and phase field method have been taken to predict the microstructure evolution in some machining processes. Li et al. [19] simulated the dynamic recrystallization process in solder interconnections by using MC method. The MC model is based on the energy minimization principle, however, the nucleation and growth of the dynamic recrystallization grains are not well considered. Takaki et al. [20] simulated the dynamic recrystallization process during the hot-working through multi-phase-field model, but the phase field method requires a large amount of computing resources, which restricts its application. The CA method has advantages in simulating the microscopic behavior of material. The CA method is a mathematical algorithm that is based on the principle of biological cell self-replication, it can be used to describe the evolution of complex system based on simple transformation rules, the transformation rules can be determined according to the physical mechanism of specific objects [21]. Meanwhile, the CA method has high efficiency and low cost, so that it has wide application. Many scholars have used the CA method to simulate the grains' nucleation and growth processes. Chen et al. [22] predicted the microstructural evolution process of magnesium alloy during hot deformation using CA method. Kühbach et al. [23] used 3D CA microstructure model to simulate the grain distribution of primary recrystallization. In recent years, the CA model is combined with FE method to simulate the evolution process of microstructures. Zhang et al. [24] used finite element - cellular automaton (FE-CA) model to predict the thermal history and grain morphology of Ti-6Al-4V. Wu et al. [25] simulated the discontinuous dynamic recrystallization of IMI834 alloy during isothermal hot compression process through FE-CA method. In this study, the temperature, stress and strain fields obtained from the FE model are used to calculate the nucleation rate, dislocation density etc. of the dynamic recrystallization in CA simulation processes, so that the CA model can simulate the dynamic recrystallization process based on the formation mechanism of the white layer. It can be seen from previous studies that the dynamic recrystallization has great influence on the white layer formation. Therefore, the emphasis of this study is to investigate the change laws of the grain size in the white layer under the influence of the dynamic recrystallization mechanism. The experiments were carried out by orthogonal cutting AISI 52100 hardened steel using PCBN inserts. The machined surfaces were analyzed under scanning electron microscopy (SEM) and X-Ray diffraction (XRD) to investigate the microstructure and grain size in the white layer. The SHPB experiments and quasi-static compression tests were conducted to obtain the true stress-true strain curves of the hardened AISI 52100 steel. A FE-CA model was developed to simulate the dynamic recrystallization process in the white layer under different cutting parameters. The effects of cutting speed and flank wear on the grain size in the white layer were discussed as well.

2. Experiments

2.1 Dry hard cutting experiments

Tubular specimens made of AISI52100 steel were cut on a MULTUS B400-W machining center. The outside diameter of the specimen is Ø88 and the wall thickness is 2 mm. the AISI52100 steel was chosen in the experiments because of its hardenability and wide application. The heat treatment process of AISI52100 is heating to 850 °C and holding for 2 hours, quenching in oil, then tempering at 280 °C for 4 hours. The average hardness of the workpieces after heat treatment is 55HRC, the microstructure of the workpieces is composed of martensite, carbide and retained austenite. The orthogonal cutting experiments were carried out using PCBN inserts. The schematic diagram of the experimental process is shown in Fig. 1. In order to improve the strength of the tool and prevent the breakdown of the cutting edge, the negative rake angle is

chosen in the cutting experiments and the parameters of the inserts are: Negative rake angle (γ_0) -10°, relief angle (α) 7°. Owing to the poor impact resistance of PCBN inserts, the negative chamfer was ground to improve the tool life and the parameter is $b_{\gamma 1}\times\gamma_{01}$ = 0.05 mm×(-20°). Three sets of cutting speed 200 m/min, 250 m/min, 350 m/min and flank wear 0 mm, 0.1 mm, 0.2 mm were chosen and the feed rate is 0.1 mm/rev. The specimens after cutting experiments were cut into small pieces for microscopic observation. The prepared samples were observed in optical microscopy and SEM to obtain the microstructure and thickness of the white layers. The grain size in the white layers under different flank wear was explored by XRD.

2.2 Dynamic compression experiments

Dry hard cutting is a process of high temperature, high strain, high strain rate. The split Hopkinson pressure bar (SHPB) experiment is widely used to obtain the mechanical properties of materials at high strain rate, so that the dynamic mechanical properties of the hardened AISI52100 steel under high temperature, high strain rate were measured by SHPB. The quasi-static mechanical property test of the hardened AISI52100 steel was carried out on the electronic universal testing machine.

Fig. 2 shows the schematic diagram of the SHPB experiments. The impact bar is impacted by air gun and impacts on the incident bar, which can generate the incident wave in the incident bar. When the incident wave propagates to the interface between the incident bar and the specimen, a part of the incident wave is reflected to the incident bar forming reflection wave, the other part passes through the specimen and propagates to the transmission bar to form the transmission wave. Fig. 3 is the wave transmission principle diagram, ε_I , ε_R and ε_T are the strain amplitude of the incident wave, reflection wave and the transmission wave, respectively.

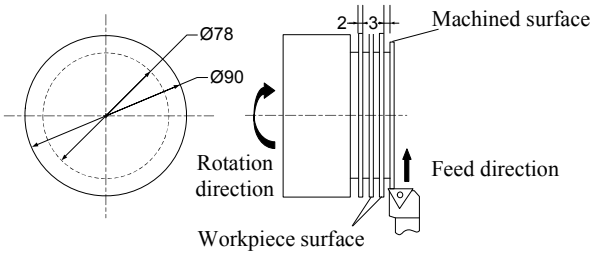

Fig. 1. The schematic diagram of the experimental process.

According to the one-dimensional stress wave theory, the strain rate, the strain and the stress can be calculated by the following Eqs.:

$$\dot{\varepsilon}(t) = -\frac{2C_0}{l}\varepsilon_R(t) \tag{1}$$

$$\varepsilon(t) = -\frac{2C_0}{l}\int_0^t \varepsilon_R(t)dt \tag{2}$$

$$\sigma = E\frac{A_0}{A_S}\varepsilon_T(t) \tag{3}$$

where $\dot{\varepsilon}$ is the strain rate, ε is the strain, σ is the stress, C_0 is the elastic wave velocity, l is the length of the specimen, E is the Young's modulus, A_0 is the cross-sectional area of the pressure bar, A_S is the cross-sectional area of the specimen.

The hardness of the AISI52100 steel in the compression experiments is 55 HRC. The size of the samples used in the SHPB experiments is Ø2×2. Four sets of temperature 20 °C, 300 °C, 500 °C, 800 °C and three sets of strain rate 3000 s^{-1}, 6000 s^{-1}, 8000 s^{-1} were carried out in the SHPB experiments. The size of the samples used in the quasi-static test is Ø4×4 and the strain rate is 1.6×10-3 s^{-1}. As soon as the SHPB experiment was over, the specimens were cooled rapidly in order to reserve the microstructure in the specimens obtained by the compression experiments. Then the specimens were etched by 4 % picric acid and observed under the optical microscopy to obtain the dynamic recrystallization grains in the specimens.

Fig. 4 shows the true stress-strain curve of the hardened AISI52100 steel under quasi-static state. Fig. 5 shows the true stress-strain curves of the hardened AISI52100 steel at different strain rate and temperature.

3. Simulation modeling

3.1 Dynamic recrystallization critical temperature

Dynamic recrystallization critical temperature can be derived from dynamic recrystallization critical strain. However, the dynamic recrystallization critical strain is difficult to be determined from the true stress-strain curves directly. The strain hardening rate θ is a parameter that can characterize the change rate of stress with strain, which is described as follows:

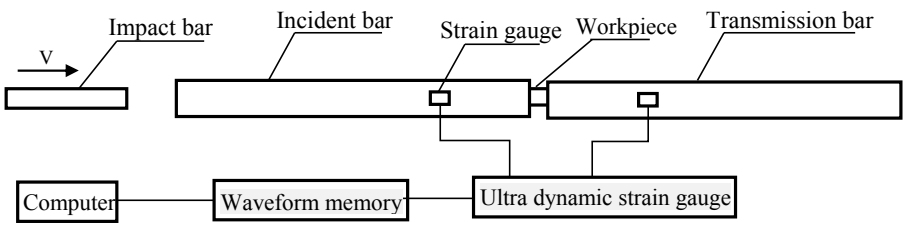

Fig. 2. Schematic diagram of SHPB experiments.

$$\theta = d\sigma / d\varepsilon \tag{4}$$

where σ is the true stress, ε is the true strain.

Poliak and Jonas proposed that the critical condition of the dynamic recrystallization is related to the inflection point of the $\theta - \sigma$ curve [26], the σ corresponding to the inflection point of the $\theta - \sigma$ curve is the critical stress of dynamic recrystallization. As shown in Eq. (4) that θ can be obtained through calculating the slope of the true stress - strain curve. The inflection point of the $\theta - \sigma$ curve can be calculated as follows:

$$-\frac{d\theta}{d\sigma} = -d(\frac{d\sigma}{d\varepsilon}) / d\sigma \,. \tag{5}$$

The $-d\theta / d\sigma - \sigma$ curve is shown in Fig. 6, the stress corresponding to the lowest point of the curve is the critical stress σ_c of the dynamic recrystallization, and the corresponding strain value of the critical stress is the critical strain ε_c.

ε_p is the peak strain which can be read directly from the true stress-strain curve, the relationship between ε_c and ε_p is that:

$$\varepsilon_c = k_0 \varepsilon_p \tag{6}$$

where k_0 is constant.

ε_p can be described as follows [27]:

$$\varepsilon_p = a_1 \dot{\varepsilon}^{m_0} \exp(Q / RT) \tag{7}$$

$$\ln \varepsilon_p = \ln a_1 + m_0 \ln \dot{\varepsilon} + Q / RT \tag{8}$$

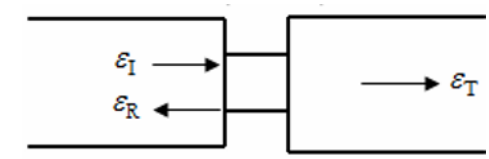

Fig. 3. Wave transmission principle diagram.

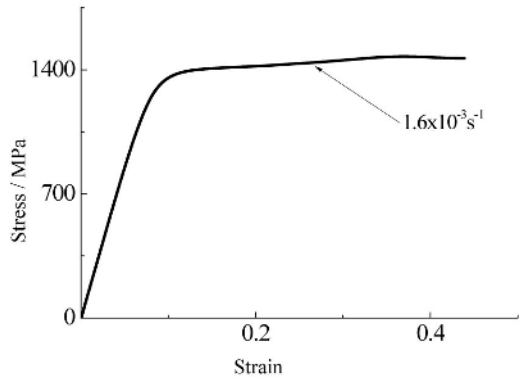

Fig. 4. True stress-strain curves under quasi-static state.

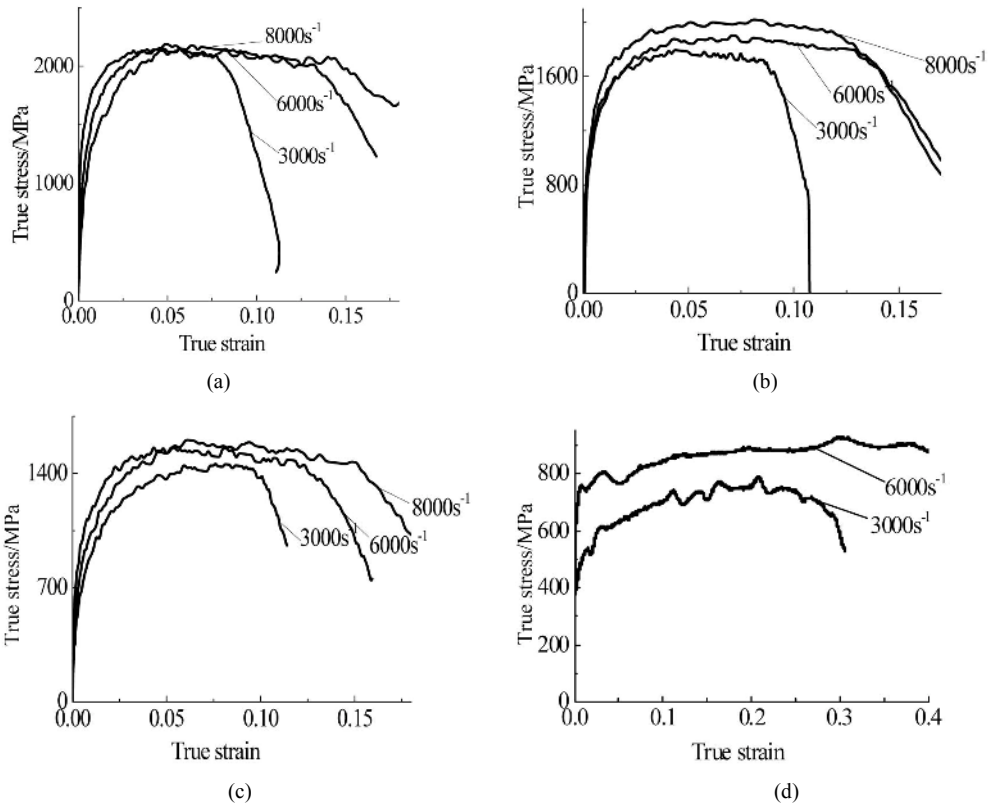

Fig. 5. True stress-strain curves of hardened AISI 52100 steel: (a) T = 20 °C; (b) T = 300 °C; (c) T = 500 °C; (d) T = 800 °C at different strain rates.

Table 1. Parameters of the dynamic recrystallization critical temperature function.

Q (J/mol)	m	k_1	a_1
-17315	0.69984	0.4135	0.00573

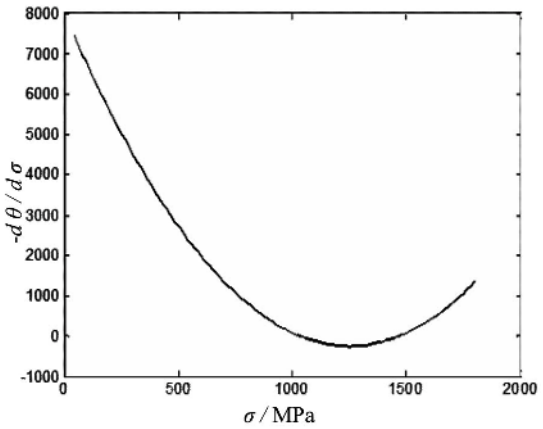

Fig. 6. $-d\theta / d\sigma - \sigma$ curve.

where Q is the thermal deformation activation energy, R is the gas constant, a_1 and m_0 are constants.

Finally, the dynamic recrystallization critical temperature under high temperature and high strain rate can be expressed as follows:

$$T_{DRX} = \frac{Q}{R(\ln \varepsilon_c - m_0 \ln \dot{\varepsilon} - \ln k_0 - \ln a_1)}. \quad (9)$$

The parameters in the Eq. (9) can be fitted by regression analysis method and are shown in Table 1.

3.2 FE modeling

The Johnson-Cook (J-C) model can describe the relationship between temperature, stress, strain and strain rate of material, and can reflect the strain hardening, strain rate hardening and temperature softening of material under high strain rate. Therefore, the J-C model is suitable to describe the hard cutting process. The flow stress expressed by the J-C model is described as follows:

$$\sigma = \left[A + B\varepsilon^{n}\right]\left[1 + C\ln\left(\frac{\dot{\varepsilon}}{\dot{\varepsilon}_0}\right)\right]\left[1 - \left(\frac{T - T_r}{T_m - T_r}\right)^{m}\right] \quad (10)$$

where σ is flow stress, ε is plastic stain, $\dot{\varepsilon}$ is plastic strain rate, $\dot{\varepsilon}_0$ is reference strain rate, A is initial yield stress, B is strain hardening coefficient, C is strain rate hardening coefficient, n is strain hardening exponent, T_r is reference temperature, T_m is melting temperature of material, m is thermal softening coefficient. The compression rate of the quasi-static compression test is 0.5 mm/min, so that the reference strain rate $\dot{\varepsilon}_0$ is $1.6\times10^{-3}s^{-1}$. A can be obtained from the true stress-strain curve that is measured by the quasi-static test under normal temperature. B, C, n, m can be calculated by regression analysis method based on the true stress- true strain curves of the AISI52100 steel as shown in Fig. 5. Table 2 shows the calculated J-C model parameters of the AISI52100 steel with the hardness of 55HRC.

Table 2. J-C model parameters of AISI52100 steel (55HRC).

Parameter	A (MPa)	B (MPa)	C	n	m
Value	1670	283	0.01638	0.40795	0.87987

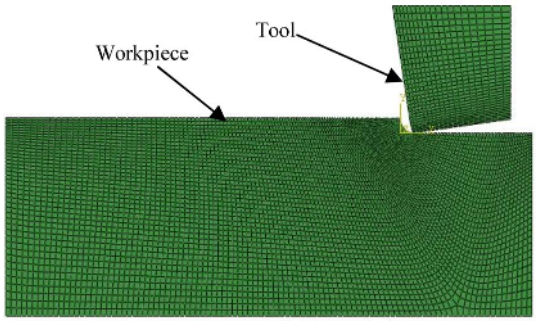

Fig. 7. FE model of the orthogonal cutting.

Dry hard cutting is a process of large strain, high strain rate and ABAQUS software has unique advantages in multi field coupling and nonlinear analysis, so that the ABAQUS software was chosen to simulate the dry hard cutting process.

The constitutive equation used in the simulation process is J-C model. Arbitrary Lagrange Euler (ALE) adaptive mesh generation method was adopted because ALE can solve the problem of mesh distortion. Modified Coulomb friction model was used to describe the state of interface friction during the cutting simulation and the expression is shown as follows:

$$\begin{cases} \tau_f = \mu\sigma_n & \text{when } \mu\sigma_n < \tau_p \\ \tau_f = \tau_p & \text{when } \mu\sigma_n \geq \tau_p \end{cases} \quad (11)$$

where τ_f is frictional stress in contact surface, μ is the friction coefficient in sliding region, σ_n is normal stress in contact surface, τ_p is the critical shear yield stress of material.

An FE model of two-dimensional orthogonal cutting is established based on ABAQUS/Explicit™ as shown in Fig. 7. Four-node bilinear displacement and temperature quadrilateral (CPE4RT) element was applied on both the workpiece and the tool. The number of nodes of the workpiece and the tools are 5496 and 620, respectively. The workpiece material, tool material, tool parameters and cutting parameters in the simulation are all same as those in the cutting experiments. The physical properties of the AISI52100 steel are shown in Table 3.

Table 3. Physical properties of the AISI52100 steel [18].

Temperature (°C)	Young's modulus (GPa)	Poisson's ratio	Expansion ($\times 10^{-6}$/°C)	Conductivity (W /(m°C))
22	201.0	0.277	11.5	52.5
200	179.0	0.269	12.6	47.5
400	163.0	0.255	13.7	41.5
600	103.0	0.342	14.9	32.5
800	86.9	0.396	15.3	26.0
1000	67.0	0.490	15.3	29.0
1500	-	-	14.9	30.0
Temperature (°C)	Specific heat (J (kg/°C))	Density (kg /m^3)		
25	458	7827		
200	640			
430	745			
540	798			

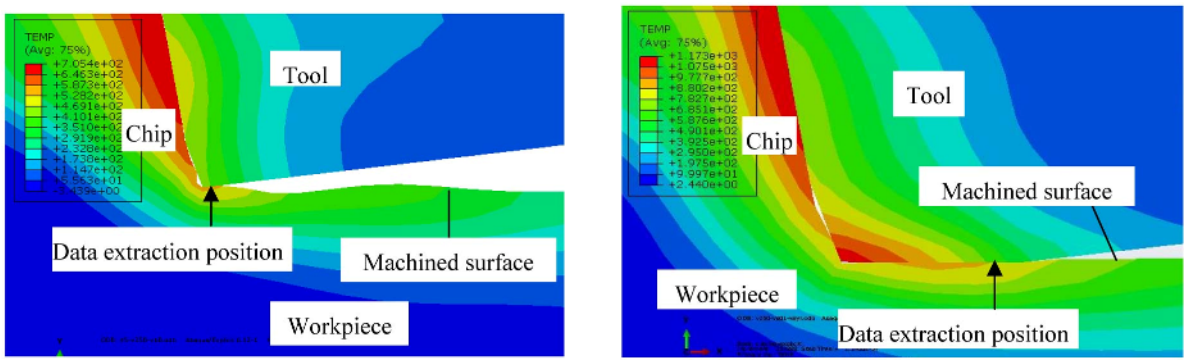

(a) (b)

Fig. 8. Data extraction method of temperature and strain in FE modeling: (a) For tools without flank wear; (b) for tools with flank wear.

As the dynamic recrystallization process is significantly influenced by temperature and strain, the temperature and strain field of the white layer are extracted from the FE simulation results and would be applied to the simulation of the dynamic recrystallization process in the white layer based on the CA model. The dynamic recrystallization critical temperature was calculated by importing the simulated stress and strain data into the Eq. (9) and the calculated result shows that the critical temperature is less than 500 °C. The temperature of the workpiece at the depth of 5 μm from the machined surface is over 500 °C, so that the dynamic recrystallization occurs at the depth of 5 μm from the machined surface. The temperature and strain distribution of the machined surface and subsurface are different at different cutting parameters. To provide accurate data for the CA model, the temperature and strain data were extracted from three positions where the depth to the machined surface is 1 μm, 3 μm and 5 μm. The extraction modes of the temperature and strain data are divided into two cases: one is extracted from the bottom of the tool tip when the tool has no flank wear as shown in Fig. 8(a). The highest temperature and strain in the machined surface exist at the bottom of the tool tip. The other is extracted from the end of the flank wear when the tool has flank wear as shown in Fig. 8(b). The highest temperature and strain in the machined surfaces is at the end of the flank wear as the result of severe extrusion and friction between the tool and the machined surface, so that the data were extracted from the end of the flank wear.

3.3 CA modeling

The dynamic recrystallization process in the white layer consists of grain nucleation process and grain growth process, the grain nucleation and grain growth process are closely related to the dislocation density of the material. Therefore, the dynamic recrystallization model in the white layer consists of four parts: Substrate formation model, dislocation density model, dynamic recrystallization grain nucleation model, dynamic recrystallization grain growth model. Two assumptions are made to simplify the CA model:

(1) The initial dislocation density in the substrate is uniform and the nucleation of the dynamic recrystallization grains does not occur until the dislocation density reaches the critical value. The dislocation density in the new dynamic recrystalli-

zation grains is zero and increases with the increase in strain. The dislocation density of the dynamic recrystallization grains increases with the strain.

(2) The nucleation sites of the dynamic recrystallization grains are in the grain boundaries of the substrate and the dynamic recrystallization area, no dynamic recrystallization nucleation occurs inside the substrate.

To simplify the model, it is assumed that the grain shape of the substrate is round, the Eq. (12) can be used to calculate the grain size of the substrate:

$$N\mathrm{L}_0^{\ 2} = \dot{N}\pi(\frac{D_0}{2})^2 \tag{12}$$

where N is the number of the cells, L_0 is the side length of the cellular; $\dot{N}$ is the nucleation rate, D_0 is the grain size of the substrate. Therefore, the grain size of the substrate can be expressed as follows:

$$D_0 = 2L\sqrt{N/(\dot{N}\pi)}\ . \tag{13}$$

The grain size of the substrate should be consistent to that of AISI52100 by changing the nucleation rate $\dot{N}$. The grain size of AISI52100 can be observed by the optical microscopy.

The nucleation rate of the dynamic recrystallization can be expressed as follows [28]:

$$\dot{N}(\dot{\varepsilon},T)=C\dot{\varepsilon}^{\mathrm{m}}\exp(-\frac{Q_a}{RT}) \tag{14}$$

where $\dot{N}$ is the nucleation rate, C is constant, Q_a is the deformation activation energy, R is the ideal gas constant, T is the deformation temperature. The temperature data extracted from the FE simulation results would be read into Eq. (14) and are used to calculate the nucleation rate under different cutting parameters. In this model, when the dislocation density in the substrate reaches to the critical dislocation density, the nucleation process begins to occur at grain boundaries.

The critical dislocation density of the dynamic recrystallization is given as follows [28]:

$$\rho_{\mathrm{c}}=\left(\frac{20\gamma\dot{\varepsilon}}{3\mathrm{bL}M\tau^2}\right)^{1/3} \tag{15}$$

where ρ_c is the critical dislocation density, γ is the grain boundary energy, b is the burgers vector; L is the average dislocation free energy, M is the grain boundary mobility, τ is the line dislocation that can be expressed as follows:

$$\tau = c_2\mu_s b^2 \tag{16}$$

where c_2 is constant, μ_s is shear modulus of material.

The average dislocation free energy L can be calculated by the following equation:

$$K=\frac{\sigma L}{\mu_s \mathrm{b}} \tag{17}$$

where K is constant and the value is 10 when the material is AISI52100 steel.

The average dislocation density during the dynamic recrystallization process can be described as follows [29]:

$$\frac{\mathrm{d}\rho}{\mathrm{d}\varepsilon}=k_1\sqrt{\rho}-k_2\rho+\frac{1}{\mathrm{bd}} \tag{18}$$

where ρ is dislocation density, d is the average grain size of the material; k_1 , k_2 are constants, k_1 represents effect of processing hardening on dislocation density and k_2 represents effect of dynamic softening on dislocation density.

The dynamic recrystallization grains growth rate is expressed as follows [30]:

$$V=MF/(4\pi\mathrm{r}^2) \tag{19}$$

where V is the grain growth rate, F is the driving force for grain growth, M is the grain boundary mobility rate. The grain boundary mobility rate M can be calculated by following equation [26]:

$$M=\frac{\delta D_{ob}b}{kT}\exp(-\frac{Q_b}{RT}) \tag{20}$$

where k is the Boltzmann constant, b is the burgers vector, Q_{b} is self-diffusion activation energy of grain boundary, R is ideal gas constant, T is deformation temperature, δ is the grain boundary thickness of material, D_{ob} is grain boundary self-diffusion coefficient at absolute zero. The temperature data extracted from FE model would be read into Eq. (20) to calculate the value of M. The driving force for the grain growth can be described as follows [31]:

$$F=4\pi r^2\tau(\rho_m-\rho)-8\pi r\gamma \tag{21}$$

where ρ_m is the dislocation density of base metal, γ is grain boundary energy. Table 4 shows material parameters of the AISI52100 steel which are needed for simulation.

The programming software MATLAB was used to calculate the CA model as the result of its strong computing capability. The CA model consists of four parts: Cellular, cellular space, neighbor and transformation rules. The two dimensional space CA model was used in the study. The square cells were chosen in the model, the length of every cell is 1 μm and the simulation area is 400 μm×400 μm. The neighbor type of the CA model is Moore neighbor, which is shown in Fig. 9. The periodic boundary condition was used in the CA model. Each cell were given three state variables, including: Crystal orientation variable, dislocation density variable and grain boundary variable. The state variable of the crystal orientation

Table 4. Material parameters of AISI52100 steel.

Burgers vector (b /m)	Shear modulus (μ /Pa)	Deformation activation energy Q_a (KJ/mol)	Boundary self-diffusion coefficient D_{ob} (m^3/s)	Grain boundary energy γ (J/m^2)
2.58e-10	8.2e+10	43.54	0.135	0.625

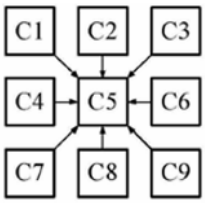

Fig. 9. Type of Moore neighbor.

ranges from 0 to 180. All cells have the same initial value of dislocation density. The dislocation density of every cell is calculated by Eq. (18). The grain boundary variable is used to represent the location information of the cells in grain boundaries. The transformation rules of the dynamic recrystallization process are based on the nucleation, dislocation density and growth models. It can be seen from Fig. 9 that the state of center cell C5 at time t+1 is determined by states of (C1, C2, C3, C4, C6, C7, C8, C9) at time t:

$$\xi_{t+1}(C_5) = f_t\begin{Bmatrix}\xi_t(C_1),\xi_t(C_2),\xi_t(C_3),\xi_t(C_4),\\ \xi_t(C_6),\xi_t(C_7),\xi_t(C_8)\end{Bmatrix}. \quad (22)$$

In order to explain the simulation process in detail, a flowchart of the CA simulation process combined with FE model is given in Fig. 10. First, the substrate is formed using the CA model. Then, the strain and cutting temperature of the hard cutting process are extracted from the FE model and are read into the CA model. The extracted strain and cutting temperature are the critical strain ε_c and the deformation temperature T of the dynamic recrystallization. Next, the dislocation density ρ of each cell is calculated based on Eq. (18), if $\rho > \rho_c$, the nucleation rate is calculated according to Eq. (14). Based on the models of the nucleation rate and growth rate, the dynamic recrystallization grains nucleate and grow at grain boundaries until the strain increment $\varepsilon > \varepsilon_c$. In this study, the temperature and strain of the subsurface with the same depth from the machined surface are the same under certain cutting parameter. Therefore, the temperature and strain data of all the cells are the same in each CA simulation process. The dynamic recrystallization process in the white layer under different cutting parameters are simulated through the CA model.

4. Results and discussion

In order to validate the accuracy of the dynamic recrystallization CA model, the microstructure of the specimens obtained from the SHPB experiment is compared with the result

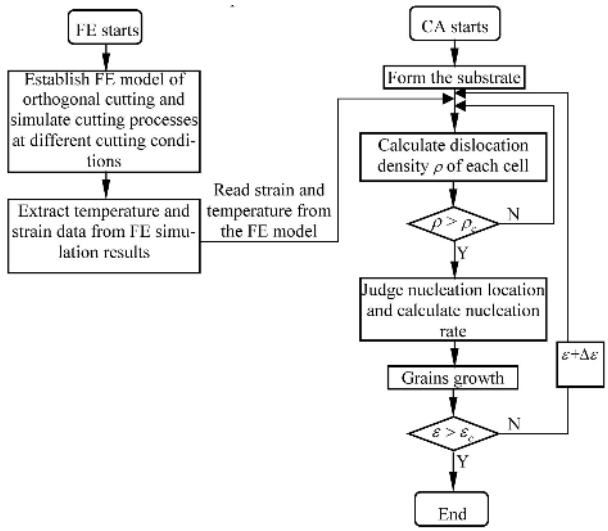

Fig. 10. Flowchart of the CA model combined with the FE model.

simulated by the CA model under the same cutting parameter. Fig. 11 shows the comparison of the dynamic recrystallization grains between the simulation and experimental results, the temperature is 300 °C and the strain rate is 4000 s^{-1}. The average grain size of the experiments and the simulation results are approximately 14.1 μm and 15.2 μm, respectively, the error between the simulation and the experiment is 7.8 %. Therefore, the developed CA model is accurate to simulate the process of dynamic recrystallization.

Fig. 12 shows an optical microscopy image of the machined surface after hard cutting. It can be seen from Fig. 12 that the machined surface is composed of the white layer, the transition layer and the substrate, the microstructure of the white layer has been significantly refined during cutting process and the grain size in the white layer is smaller than that in the transition layer and the substrate. The strong plastic deformation and high cutting temperature can be produced during the cutting process, which leads to the occurrence of dynamic recrystallization. The microstructure and grains in the white layer are refined by the dynamic recrystallization process. Fig. 13 shows the SEM images of the white layer at different cutting parameters. It can be seen from Fig. 13 that the white layer thickness is approximately 4 μm ~ 6 μm and increases with the cutting speed and the flank wear. The grain size in the white layer can be calculated by XRD patterns and the grain size of the white layer under different flank wear when v = 350 m/min, f = 0.1 mm/rev is shown in Table 5. It can be seen from Table 5. that the grain size of the white layer decreases with the increase in flank wear.

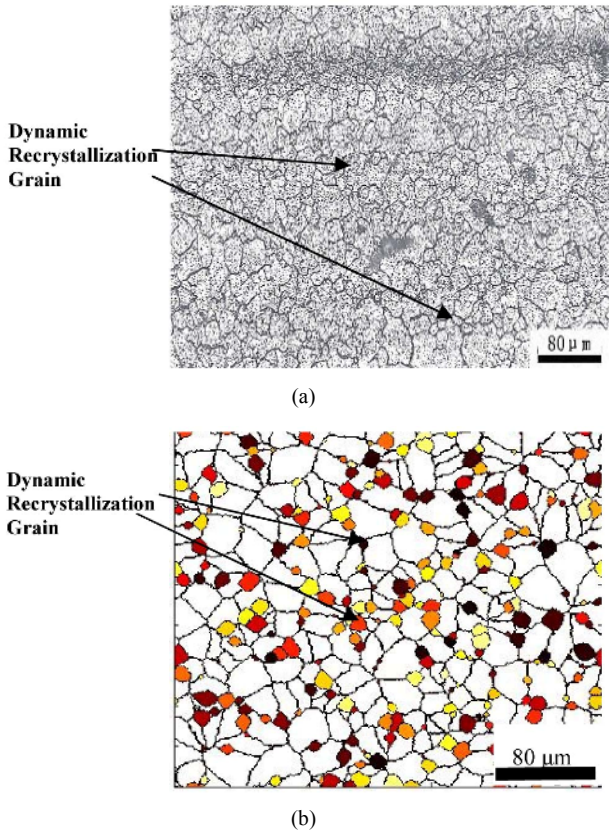

Fig. 11. Comparison of dynamic recrystallization grains between (a) experimental result; (b) simulation result of AISI52100 steel.

Fig. 14 shows the FE simulation results of the stress field with different flank wear when the cutting speed is 250 m/min. Figs. 15 and 16 show the temperature and strain data in the machined surface and the subsurface at different cutting conditions. It can be seen that the temperature and strain in the machined surface increase with the cutting speed and flank wear and the temperature and strain gradually decreases when the extraction position is away from the machined surface. These temperature and strain data were used in the CA simulation.

The dynamic recrystallization processes under different cutting speed and flank wear were simulated through the FE-CA model, and the average grain sizes of the dynamic recrystallization in the white layers under different cutting parameters were obtained from the simulation results. Fig. 17 shows the comparison of the grain size between experimental and simulation results under different flank wear when cutting speed is 350 m/min, the simulation results are the grains at the distance of 1 μm below the machined surface. It is noted that the grain size of the simulations are respectively 47 nm, 45 nm and 25 nm when VB is 0 mm, 0.1 mm, 0.2 mm, while the experimental results are 52.2 nm, 49.1 nm and 21.9 nm under the same cutting parameters, the errors between the simulations and the experiments are 10 %, 8.4 %, 12.4 % when VB is 0 mm, 0.1 mm, 0.2 mm. It can be seen from the comparison

Table 5. Grain size in the white layer under different flank wear.

Cutting parameters (v = 350 m/min, f = 0.1 mm/rev)	Sub-grain size (nm)
VB = 0	52.2
VB = 0.1 mm	49.1
VB = 0.2 mm	21.9

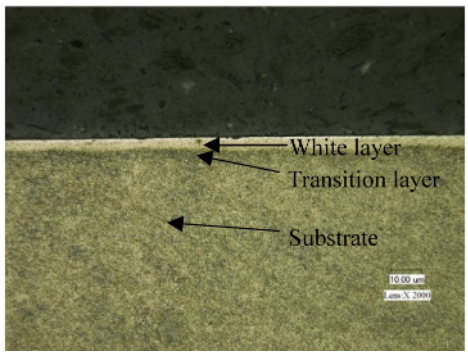

Fig. 12. Optical microscopy image of the machined surface after hard cutting.

results that the FE-CA model can simulate the dynamic recrystallization occurred in the white layer formation process accurately.

Fig. 18 shows the grain simulation results of the dynamic recrystallization where the depth from the surface is 1 μm, 3 μm and 5 μm when flank wear is 0 mm. The dynamic recrystallization grains nucleate and grow at the grain boundaries, moreover, the nucleation sites of the dynamic recrystallization grains are random, this is consistent with the actual nucleation process of the dynamic recrystallization. The results demonstrate that the dynamic recrystallization process simulated by the CA model conforms to the formation mechanism of the dynamic recrystallization in the white layer. Meanwhile, it can be seen that the cutting conditions have effects on the grain size of the dynamic recrystallization grains in the white layer, the specific influence rules are shown in Fig. 19. Fig. 19 shows the grain size in the white layer at different cutting conditions. It can be seen that the cutting speed has great influence on the grain size, the grain size decreases with cutting speed. The cutting temperature increases with the increase in cutting speed during cutting process and the dislocation motion is sensitive to temperature extremely. The movement and annihilation of dislocations are easier to process under high temperature, which accelerates the nucleation and growth of the dynamic recrystallization grain. So that the grain refinement is more obvious with the increase in cutting speed. In addition, it can be seen from Fig. 19 that the grain size in the white layer decreases with the flank wear. The friction and extrusion between the tool and the workpiece increase with flank wear, which leads to severe plastic deformation in the machined surface. The stress, strain and dislocation density in the machined surface increase with plastic deformation, which

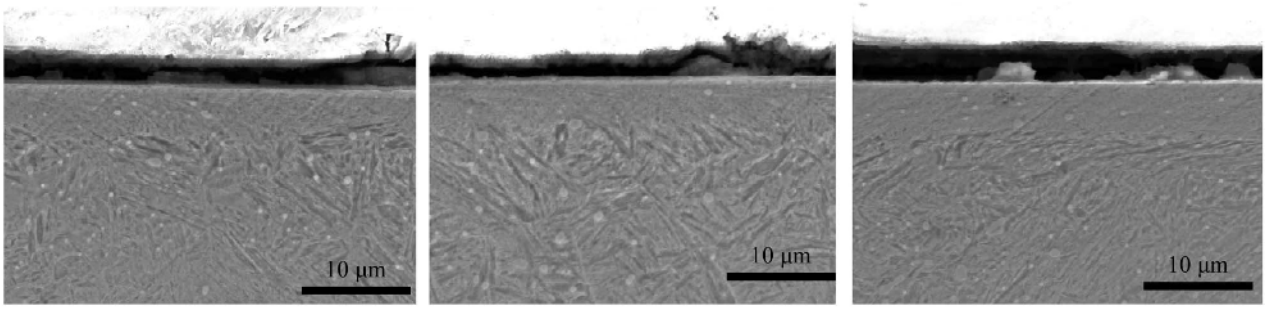

(a) (b) (c)

Fig. 13. SEM images of the white layer: (a) v = 250 m/min, VB = 0.1 mm; (b) v = 250 m/min, VB = 0.2 mm; (c) v = 350 m/min, VB = 0.1 mm.

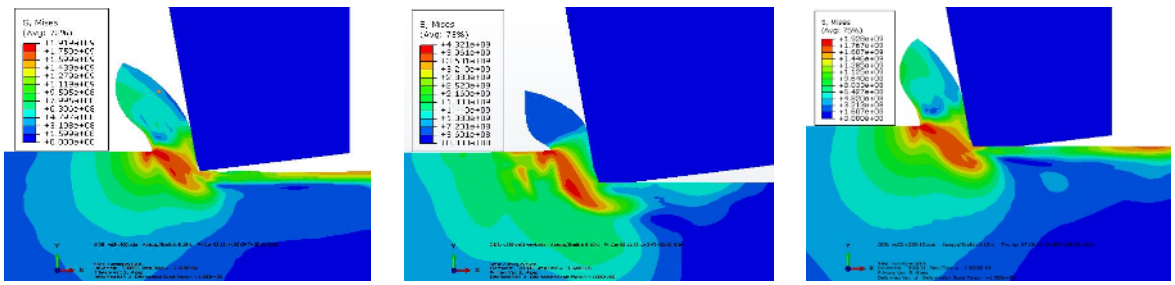

(a) VB = 0 mm (b) VB = 0.1 mm (c) VB = 0.2 mm

Fig. 14. FE simulation results of stress fields under different flank wear (v = 250 m/min).

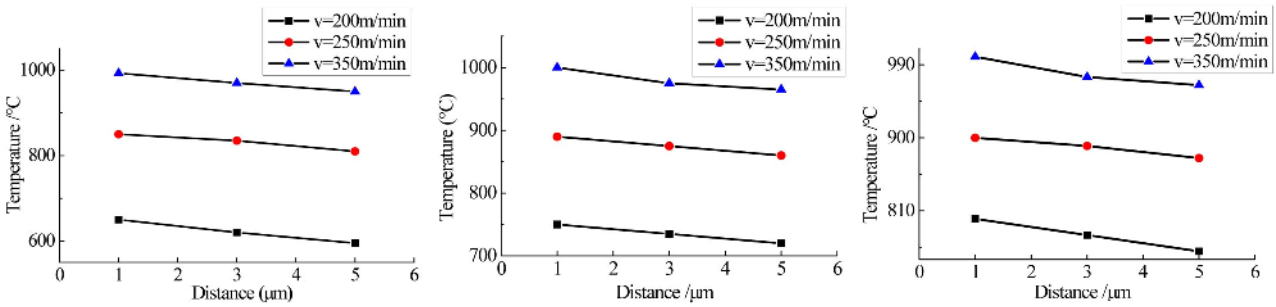

(a) (b) (c)

Fig. 15. Temperature data in the machined surface at different cutting condition: (a) VB = 0 mm; (b) VB = 0.1 mm; (c) VB = 0.2 mm.

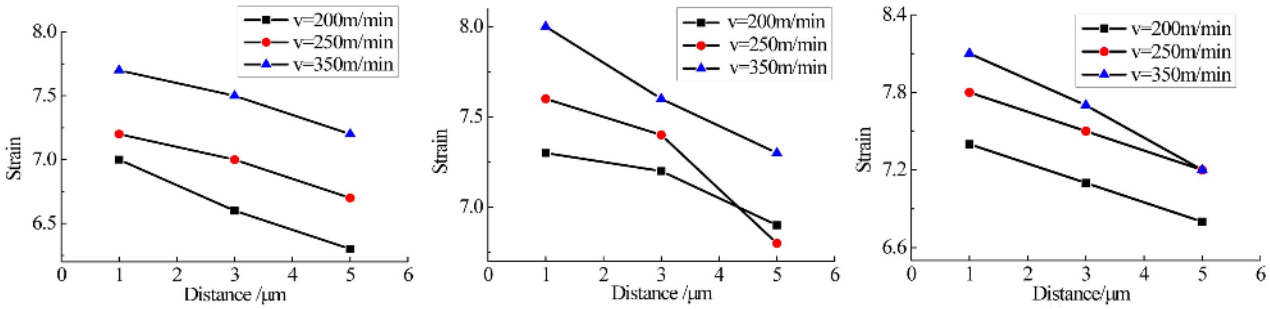

(a) (b) (c)

Fig. 16. Strain data in the machined surface at different cutting condition: (a) VB = 0 mm; (b) VB = 0.1 mm; (c) VB = 0.2 mm.

can aggravate the nucleation and growth process of dynamic recrystallization as well. The rapid nucleation and growth process lead to the decrease in the grain size in the white layer.

5. Conclusion

The FE-CA model is developed in the study to simulate the

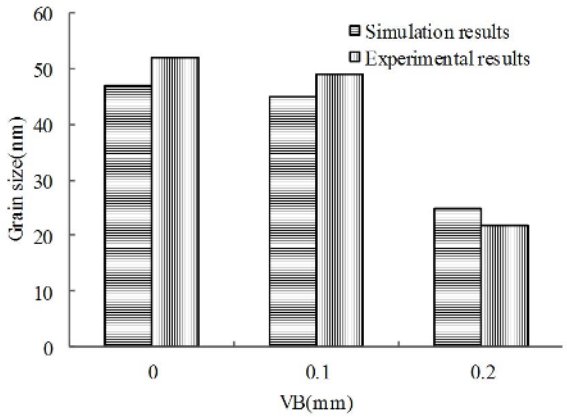

Fig. 17. Comparison of grain size in the white layer between experimental and simulation results under different flank wear (v = 350 m/min).

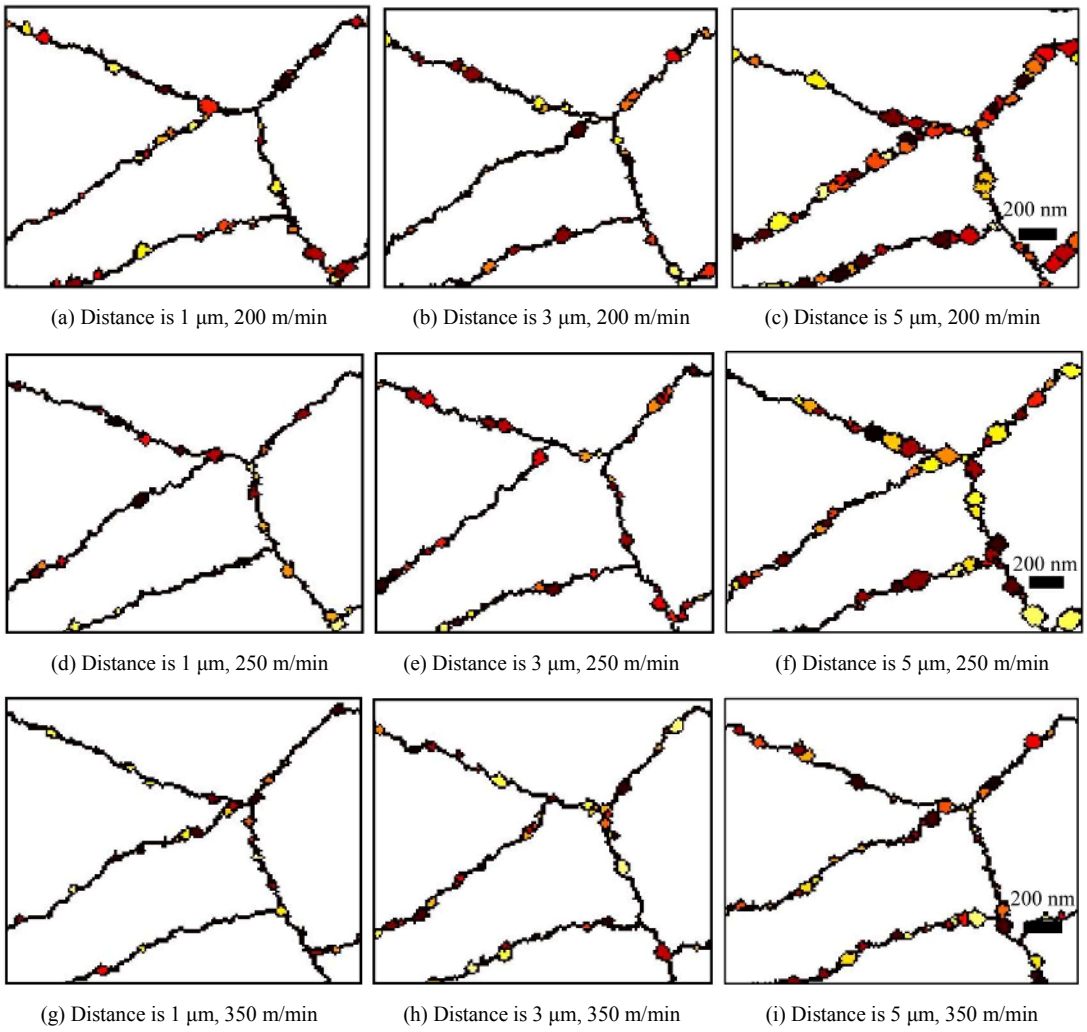

(a) Distance is 1 μm, 200 m/min (b) Distance is 3 μm, 200 m/min (c) Distance is 5 μm, 200 m/min

(d) Distance is 1 μm, 250 m/min (e) Distance is 3 μm, 250 m/min (f) Distance is 5 μm, 250 m/min

(g) Distance is 1 μm, 350 m/min (h) Distance is 3 μm, 350 m/min (i) Distance is 5 μm, 350 m/min

Fig. 18. Grains simulation of dynamic recrystallization in white layer.

dynamic recrystallization process in the white layer in hard cutting, the main content and conclusions are as follows:

The FE model is set up based on the J-C constitutive model to obtain the temperature and strain in hard cutting process. The dynamic recrystallization critical temperature model under high temperature and high strain rate is established based on the true stress-strain curves of the AISI52100 steel obtained by the SHPB experiments to confirm the dynamic re-

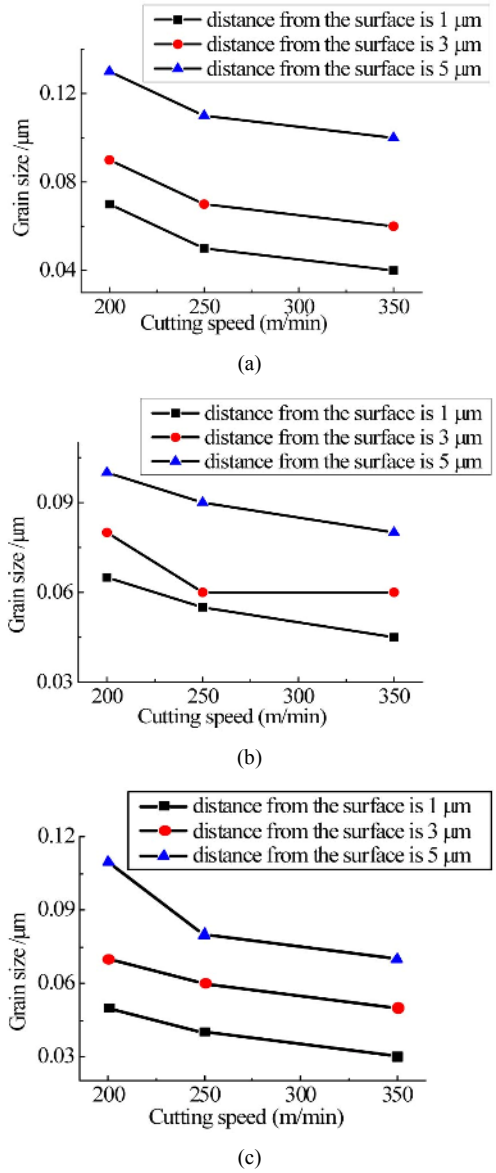

Fig. 19. Grain size in the white layer at different cutting conditions: (a) VB = 0 mm; (b) VB = 0.1 mm; (c) VB = 0.2 mm.

crystallization critical temperature in hard cutting process. The CA model is developed to simulate the dynamic recrystallization process in the white layer, so that the dislocation density model, dynamic recrystallization grain nucleation model and the dynamic recrystallization grain growth model are established in the study.

The dynamic recrystallization process is simulated by the CA model combining with the temperature and the strain data extracted from the FE simulation results. The grain size of the dynamic recrystallization obtained through the CA simulation is compared with the experimental result, and the contrast result demonstrates that the error between the simulation and experiment is less than 13 %, the FE-CA model can simulate the dynamic recrystallization process in the white layer accurately.

The dynamic recrystallization processes under different cutting speed and flank wear are simulated by the FE-CA model, results show that the grain size in the white layer decreases with the increase in cutting speed and flank wear.

Acknowledgements

This work has been supported by National Science Foundation (NO. 51375072) China and SCP (Grant No. JCKY2016 212A506-0102) China.

Nomenclature

A	: Initial yield stress
A_0	: Cross-sectional area of the pressure bar
A_S	: Cross-sectional area of the specimen
b	: Burgers vector
$b_{\gamma 1}$	: The length of negative chamfer
B	: Strain hardening coefficient
C	: Strain rate hardening coefficient
C_0	: Elastic wave velocity
d	: The average grain size of the material
D_0	: The grain size of the substrate
D_{ob}	: Grain boundary self-diffusion coefficient at absolute zero
E	: Young's modulus
f	: Feed rate
F	: Driving force
k	: Boltzmann constant
l	: The length of the specimen
L	: Average dislocation free energy
L_0	: The side length of the cellular
m	: Thermal softening coefficient
M	: Grain boundary mobility rate
n	: Strain hardening exponent
N	: Number of the cells
$\dot{N}$	: Nucleation rate
Q	: Thermal deformation activation energy
Q_a	: Deformation activation energy
Q_b	: Diffusion activation energy of grain boundary
R	: Ideal gas constant
T	: Deformation temperature
T_{DRX}	: Dynamic recrystallization critical temperature
T_m	: Melting temperature of material
T_r	: Reference temperature
v	: Cutting speed
V	: Grain growth rate
VB	: Flank wear
α	: Relief angle
γ_0	: Rake angle
γ_{01}	: Angle of negative chamfer
ε	: Strain
ε_c	: Critical strain
ε_I	: Strain amplitude of incident wave
ε_P	: Peak strain

ε_R : Strain amplitude of reflection wave
ε_T : Strain amplitude of transmission wave
$\dot{\varepsilon}$: Strain rate
$\dot{\varepsilon}_0$: Reference strain rate
σ : Stress
σ_c : Critical stress
σ_n : Normal stress in contact surface
τ : Line dislocation
τ_f : Frictional stress in contact surface
τ_p : Critical shear yield stress of material
ρ : Dislocation density
ρ_c : Critical dislocation density
ρ_m : Dislocation density of base metal
γ : Grain boundary energy
μ : Friction coefficient in sliding region
μ_s : Shear modulus of material
θ : Strain hardening rate
δ : Grain boundary thickness of material

References

[1] M. Rancic et al., Microstructural investigations of the white and deformed layers close to the turned surface of Ti-6Al-4V, *Metall. Mater. Trans. A Phys. Metall. Mater. Sci.,* 48 (1) (2017) 389-402.

[2] D. H. Cho, S. A. Lee and Y. Z. Lee, Mechanical properties and wear behavior of the white layer, *Tribol. Lett.,* 45 (1) (2012) 123-129.

[3] Y. Choi, Influence of a white layer on the performance of hard machined surfaces in rolling contact, *Proc. Inst. Mech. Eng. Part B-Journal Eng. Manuf.,* 224 (B8) (2010) 1207-1215.

[4] S. Ranganath, C. Guo and P. Hegde, A finite element modeling approach to predicting white layer formation in nickel superalloys, *CIRP Ann. - Manuf. Technol.,* 58 (1) (2009) 77-80.

[5] S. B. Hosseini et al., Formation mechanisms of white layers induced by hard turning of AISI 52100 steel, *Acta Mater.,* 89 (2015) 258-267.

[6] B. Zhang et al., Microstructures of surface white layer and internal white adiabatic shear band, *Wear,* 211 (2) (1997) 164-168.

[7] D. Umbrello, Analysis of the white layers formed during machining of hardened AISI 52100 steel under dry and cryogenic cooling conditions, *Int. J. Adv. Manuf. Technol.,* 64 (5-8) (2013) 633-642.

[8] G. Poulachon et al., An experimental investigation of work material microstructure effects on white layer formation in PCBN hard turning, *Int. J. Mach. Tools Manuf.,* 45 (2) (2005) 211-218.

[9] S. S. Bosheh and P. T. Mativenga, White layer formation in hard turning of H13 tool steel at high cutting speeds using CBN tooling, *Int. J. Mach. Tools Manuf.,* 46 (2) (2006) 225-233.

[10] S. B. Hosseini et al., Cutting temperatures during hard turning - Measurements and effects on white layer formation in AISI 52100, *J. Mater. Process. Technol.,* 214 (6) (2014) 1293-1300.

[11] S. Akcan et al., Formation of white layers in steels by machining and their characteristics, *Metall. Mater. Trans. A Phys. Metall. Mater. Sci.,* 33 (4) (2002) 1245-1254.

[12] A. Attanasio et al., Tool wear effects on white and dark layer formation in hard turning of AISI 52100 steel, *Wear,* 286-287 (7) (2012) 98-107.

[13] Y. K. Chou and H. Song, Thermal modeling for white layer predictions in finish hard turning, *Int. J. Mach. Tools Manuf.,* 45 (4-5) (2005) 481-495.

[14] G. Ambrogio et al., White and dark layer analysis using response surface methodology, *Key Eng. Mater.,* 504-506 (2012) 1335-1340.

[15] D. Umbrello and I. S. Jawahir, Numerical modeling of the influence of process parameters and workpiece hardness on white layer formation in AISI 52100 steel, *Int. J. Adv. Manuf. Technol.,* 44 (9-10) (2009) 955-968.

[16] D. Umbrello and L. Filice, Improving surface integrity in orthogonal machining of hardened AISI 52100 steel by modeling white and dark layers formation, *CIRP Ann. - Manuf. Technol.,* 58 (1) (2009) 73-76.

[17] A. Ramesh and S. N. Melkote, Modeling of white layer formation under thermally dominant conditions in orthogonal machining of hardened AISI 52100 steel, *Int. J. Mach. Tools Manuf.,* 48 (3-4) (2008) 402-414.

[18] A. Ramesh, Prediction of process-induced microstructural changes and residual stresses in orthogonal hard machining, *Georg. Inst. Technol.* (2002).

[19] J. Li et al., Simulation of dynamic recrystallization in solder interconnections during thermal cycling, *Comput. Mater. Sci.,* 50 (2) (2010) 690-697.

[20] T. Takaki et al., Multiscale modeling of hot-working with dynamic recrystallization by suffer microstructure evolution and macroscopic mechanical behavior, *Int. J. Plast.,* 52 (2014) 105-116.

[21] X. J. Guan et al., Simulation of dynamic recrystallization for advanced steel HPS485wf using cellular automata, *Trans. Mater. Heat Treat.,* 35 (6) (2014) 218-224.

[22] M. S. Chen et al., Modeling and simulation of dynamic recrystallization behaviors of magnesium alloy AZ31B using cellular automaton method, *Comput. Mater. Sci.,* 136 (2017) 163-172.

[23] M. Kühbach, G. Gottstein and L. A. Barrales-Mora, A statistical ensemble cellular automaton microstructure model for primary recrystallization, *Acta Mater.,* 107 (2016) 366-376.

[24] J. Zhang et al., A coupled finite element cellular automaton model to predict thermal history and grain morphology of Ti-6Al-4V during direct metal deposition (DMD), *Addit. Manuf.,* 11 (2016) 32-39.

[25] W. Chuan, Y. He and L. H. Wei, Modeling of discontinuous dynamic recrystallization of a near-α titanium alloy IMI834 during isothermal hot compression by combining a cellular automaton model with a crystal plasticity finite element

method, *Comput. Mater. Sci.,* 79 (2013) 944-959.
[26] E. I. Poliak and J. J. Jonas, A one-parameter approach to determining the critical conditions for the initiation of dynamic recrystallization, *Acta Mater.,* 44 (1) (1996) 127-136.
[27] J. M. Cabrera et al., Modeling the flow behavior of a medium carbon microalloyed steel under hot working conditions, *Metall. Mater. Trans. A Phys. Metall. Mater. Sci.,* 28 (11) (1997) 2233-2243.
[28] F. Chen et al., Modeling and simulation on dynamic recrystallization of 30Cr2Ni4MoV rotor steel using the cellular automaton method, *Model. Simul. Mater. Sci. Eng.,* 17 (7) (2009).
[29] H. Mecking and U. F. Kocks, Kinetics of flow and strain-hardening, *Acta Metall.,* 29 (11) (1981) 1865-1875.
[30] R. Ding and Z. X. Guo, Coupled quantitative simulation of microstructural evolution and plastic flow during dynamic recrystallization, *Acta Mater.,* 49 (16) (2001) 3163-3175.
[31] F. J. Humphreys and M. Hatherly, *Recrystallization and related annealing phenomena,* Second Edition, Elsevier (2004).

Chunzheng Duan, Associate Professor, doctoral supervisor, now is working in School of Mechanical Engineering in China. His main research direction is high speed and high efficiency cutting technology. He chaired 3 Chinese National Natural Science Foundation and published more than 50 papers.